ANNUAL REVIEWS

Annual Review of Control, Robotics, and Autonomous Systems

Robotic Micromanipulation: Fundamentals and Applications

Zhuoran Zhang,[1,*] Xian Wang,[1,2,*] Jun Liu,[1] Changsheng Dai,[1] and Yu Sun[1,2,3]

[1]Department of Mechanical and Industrial Engineering, University of Toronto, Toronto, Ontario M5S 3G8, Canada; email: zhuoran@mie.utoronto.ca, xianjeremy.wang@mail.utoronto.ca, ljun.liu@mail.utoronto.ca, chagnsheng.dai@mail.utoronto.ca, sun@mie.utoronto.ca

[2]Institute of Biomaterials and Biomedical Engineering, University of Toronto, Toronto, Ontario M5S 3G8, Canada

[3]Department of Electrical and Computer Engineering, University of Toronto, Toronto, Ontario M5S 3G8, Canada

Annu. Rev. Control Robot. Auton. Syst. 2019. 2:11.1–11.23

The *Annual Review of Control, Robotics, and Autonomous Systems* is online at control.annualreviews.org

https://doi.org/10.1146/annurev-control-053018-023755

*These authors contributed equally to this article

Keywords

robotics, micromanipulation, automation

Abstract

Robotic micromanipulation is a relatively young field. However, after three decades of development and evolution, the fundamental physics; techniques for sensing, actuation, and control; tool sets and systems; and, more importantly, a research community are now in place. This article reviews the fundamentals of robotic micromanipulation, including how micromanipulators and end effectors are actuated and controlled, how remote physical fields are utilized for micromanipulation, how visual servoing is implemented under an optical microscope, how force is sensed and controlled at the micro- and nanonewton levels, and the similarities and differences between robotic manipulation at the micro- and macroscales. We also review representative milestones over the past three decades and discuss potential future trends of this field.

1. INTRODUCTION

The invention of the microscope in the seventeenth century empowered humans to visualize the previously unknown microworld and enabled the inception of micromanipulation—for instance, the manual assembly of small parts by skilled watchmakers. It was not until the 1990s that intense efforts to develop robotic micromanipulation technologies began, enabled by several different developments: Robotic manipulation at the macroscale became more mature, the booming of microtechnologies (e.g., microfabrication) made it feasible to create precision tools for manipulating small objects, and the need to perform precision manipulation tasks in many disciplines and industries required the replacement of manual operation with automated robotic micromanipulation. **Figure 1** shows an overview of robotic micromanipulation principles and systems. Micromanipulation can be achieved with motor-driven micromanipulators or untethered physical fields (e.g., optical and magnetic fields) under optical microscopy imaging. These approaches have been used to manipulate a multitude of objects, ranging in size from submicrometers to a few millimeters.

The past three decades have witnessed tremendous advances in robotic micromanipulation, with some of the representative milestones shown in **Figure 2** (for a more detailed list, see **Table 1** in Section 5). A robotic micromanipulator with six degrees of freedom (DOFs) was first developed in the early 1990s (1). In the mid-1990s, scaling effects on micromanipulation (2, 3) and control issues for micromanipulation (4–6) were reviewed. In 1999, fundamentals of robotic micromanipulation using force fields were investigated (7), and in the early 2000s, robotic micromanipulation techniques were developed for manipulating and characterizing biological cells (8). Since 2005, a large number of mobile microrobots have been developed for micromanipulation tasks, embodied as an artificial structure (9–12), a motile microorganism [e.g., a magnetotactic bacterium (13)], and a biohybrid microswimmer (14). After 2010, the development of robotic micromanipulation systems became more targeted toward specific industry and clinical uses—for instance, to perform robotic microassembly in industry (15) and precision robotic surgery or drug delivery (16–20), with the ultimate goal of clinical deployment.

This article describes the fundamentals of robotic micromanipulation, reviews representative major events over the past three decades, and discusses potential future trends of this field. Since

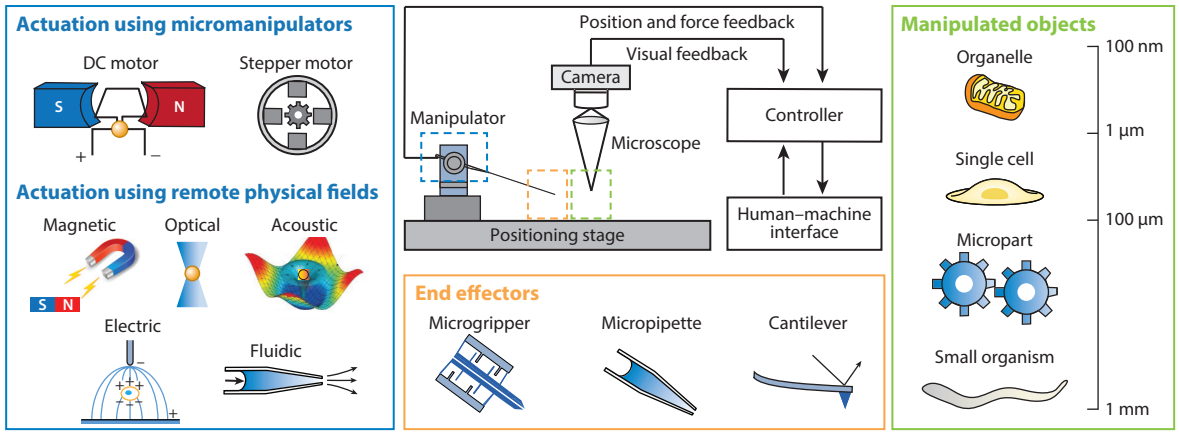

Figure 1

Robotic micromanipulation principles and systems. A robotic micromanipulation system is built around an optical microscope. Actuation is achieved by the use of micromanipulators or remote physical fields to manipulate micro-objects such as organelles (1 μm and smaller), single cells (1–100 μm), microparts (100 μm–1 mm), and small organisms (approximately 1 mm). Acoustic image adapted from Reference 74 with permission from the National Academy of Sciences.

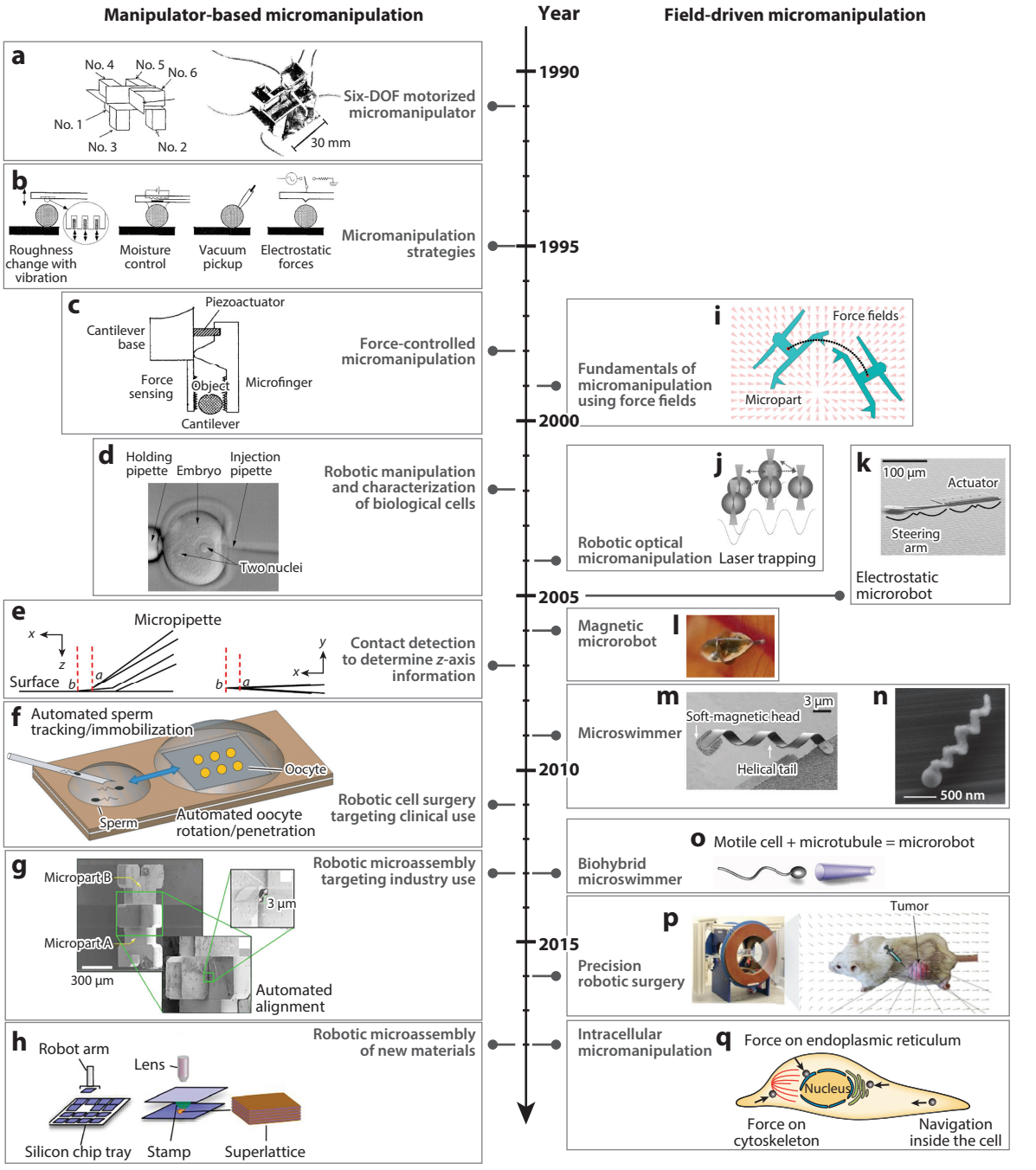

(Caption appears on following page)

Figure 2 (*Figure appears on preceeding page*)

Representative activities in robotic micromanipulation. (*Left panels*) Robotic micromanipulation using motorized micromanipulators. (*a*) A micromanipulator with six degrees of freedom (DOFs) that uses piezoelectric actuators. Panel adapted from Reference 1 with permission from IEEE. (*b*) Micromanipulation strategies utilizing scaling effects. Panel adapted from Reference 2 with permission from IEEE. (*c*) A laser-based noncontact force sensor integrated into a microgripper for force-controlled grasping of micro-objects. Panel adapted from Reference 112 with permission from IEEE. (*d*) Microrobotic systems developed to manipulate and characterize biological cells. Panel adapted from Reference 8 with permission from SAGE Publishing. (*e*) A contact detection method developed to use computer vision microscopy during manipulation to determine the *z* coordinate under an optical microscope. Panel adapted from Reference 100 with permission from SAGE Publishing. (*f*) Robotic systems that target clinical infertility treatment. Panel adapted from Reference 16 with permission from IEEE. (*g*) Robotic systems that target industrial microassembly. Panel adapted from Reference 15 with permission from Springer-Verlag. (*h*) Robotic micromanipulation for the assembly of thin 2-D crystals for new material development. Panel adapted from Reference 149 with permission from Nature Publishing Group. (*Right panels*) Robotic micromanipulation using noncontact fields. (*i*) Investigation of fundamentals of micromanipulation using programmable force fields. Panel adapted from Reference 7 with permission from SAGE Publishing. (*j*) Synchronized micromanipulation of multiple objects using laser trapping. Panel adapted from Reference 64 with permission from AIP Publishing. (*k*) A mobile microrobot actuated by electrostatic force. Panel adapted from Reference 10 with permission from IEEE. (*l*) A magnetic microrobot (fundamentals of magnetic micromanipulation were also investigated around this time). Panel adapted from Reference 11 with permission from SAGE Publishing. (*m*,*n*) Design and fabrication of artificial helical magnetic microswimmers. Panels *m* and *n* adapted from References 59 and 12 with permission from AIP Publishing and the American Chemical Society, respectively. (*o*) A motile sperm (providing propulsion) combined with a magnetic microtube (providing steering) to form a biohybrid microswimmer. Panel adapted from Reference 14 with permission from Wiley. (*p*) Drug delivery into the hypoxic region of a tumor inside a mouse using biohybrid microrobots. Panel adapted from Reference 18 with permission from Nature Publishing Group. (*q*) Control of a submicrometer magnetic bead inside a single cell for intracellular navigation and measurement. Panel adapted from Reference 56 with permission from IEEE.

the scaling of physical laws (21, 22) and the manipulation of nanoscale objects (i.e., nanomanipulation) have been extensively reviewed elsewhere (23–25), we do not discuss these topics. Instead, we focus on how micromanipulators and end effectors are actuated and controlled, how remote physical fields are utilized for micromanipulation, how visual servoing is implemented under an optical microscope, how force is sensed and controlled at the micro- and nanonewton levels, and similarities and differences between robotic manipulation at the micro- and macroscales. We also discuss representative applications and discoveries enabled by robotic micromanipulation.

2. ROBOTIC MICROMANIPULATORS AND END EFFECTORS

Micromanipulation demands micromanipulators with a submicrometer positioning resolution and a motion range of a few millimeters. This positioning resolution and motion range are necessary to manipulate objects with characteristic dimensions of micrometers and to cover a field of view under optical microscopy that is a few square millimeters or smaller. Micromanipulators driven by DC motors are closed-loop controlled with encoder feedback and can provide a repeatable positioning resolution and accuracy of 0.1 μm and motion ranges of up to a few centimeters. Although commercial stepper-motor-driven micromanipulators have a claimed positioning resolution of 0.02–0.05 μm, this is based on the theoretical positioning resolution of microstepping and is not repeatable in practice due to step loss and backlash. Piezo-driven manipulators can achieve a higher positioning resolution of nanometers but are less commonly used than DC-motor- and stepper-motor-driven micromanipulators for robotic micromanipulation since the imaging resolution of optical microscopy is typically approximately 0.2 μm, a limitation imposed by the diffraction limit of light.

These high-resolution motors form prismatic joints to provide translational motion, whereas revolute joints are not often built in micromanipulators. Since microscopes have a limited field of view and depth of field, rotation-induced translation can easily move the end effector out of the field of view and/or out of focus. With only prismatic joints, most micromanipulators are Cartesian manipulators with three prismatic joints connected in serial and orthogonal to each

Table 1 Summary of representative milestones in robotic micromanipulation

Year	Milestone	Reference(s)
1991	Robotic micromanipulator with six degrees of freedom	1
1995	Reviews of the scaling effects of physical laws on micromanipulation	2, 3
1997	Review of control issues in micromanipulation	4
1998	Additional reviews of control issues in micromanipulation	5, 6
	Force-controlled robotic micromanipulation	112
1999	Robotic parallel microassembly using programmable force fields	7
2000	Microassembly station with mobile piezoelectric microrobots	117
2002	Robotic cell manipulation	8
2004	Synchronized micromanipulation of multiple objects using laser trapping	64
2006	Microelectromechanical-system electrostatic mobile microrobots	10
	Mobile microrobots using magnetic fields	11
	On-chip micromanipulation and assembly of colloidal particles by electric fields	78
2007	Contact detection for determining z coordinates in micromanipulation	100
2009	Design and fabrication of an artificial bacterial flagellum	12, 59
2010	Hybrid microassembly combining robotic pick and place and capillary self-alignment	96
	OctoMag electromagnetic system	52
2011	Clinical robotic cell surgery for in vitro fertilization	16
	3-D assembly of microscale hydrogels	125
2013	Robotic microassembly systems for industry use	15
	Magnetically navigated catheter in cardiac electrophysiology procedures	139
	MicroStressBots driven by electrostatic forces	123
2014	Robot cell manipulation for drug testing	135
	Protein harvesting with a rolling microrobot	83
	Assembly of cell-encapsulating hydrogels	126
	In vivo wireless biopsy using a magnetically actuated soft capsule endoscope	138
	Magnetic microrobots with in situ force-sensing capabilities	109
2016	3-D acoustic tweezers for cell manipulation	74
	Drug delivery into the hypoxic region of a tumor inside a mouse using biohybrid microrobots	18
2017	In vivo micromanipulation of single cells using an optical field	69
2018	Magnetic swarm control for hyperthermia treatment of cancer cells	62
	Navigation of a submicrometer magnetic bead inside a single cell for robotic intracellular manipulation	56

other. An additional tilt axis is sometimes added to form a four-DOF micromanipulator. The tilt axis is redundant to the x and z axes but can help avoid synchronization issues in the simultaneous control of the two axes, especially for biological applications, such as microinjection (26) and patch clamp (27), where the motion of the end effector mounted on the tilt axis needs to be fast and accurately controlled.

For kinematics, having fewer DOFs of micromanipulators reduces the dimension of the transformation matrix that relates the positions of the end effector and the joints. Solving kinematics without rotational DOFs does not involve trigonometric equations, which may rely on iterative solving. A lack of rotational DOFs also means that there is no singularity in the micromanipulator's workspace because the Jacobian matrix is of full rank. Because the workspace of Cartesian

micromanipulators is cubic, it is easy to adjust the manipulator workspace to cover the field of view of the microscope. Furthermore, the inverse Jacobian matrix for the translational micromanipulators can be directly computed using the full-rank Jacobian matrix instead of the pseudoinverse matrix (28). Generally, the Jacobian matrix of Cartesian micromanipulators is a diagonal matrix, and the position of the end effector can be directly controlled by moving each independent axis of the micromanipulator.

End effectors are tools mounted on a micromanipulator to interact with micro-objects for tasks such as pick and place. Microgrippers and single-ended probes [e.g., micropipettes and atomic force microscopy (AFM) probes] are typical end effectors used in robotic micromanipulation. Microgrippers have finger openings that typically range from several micrometers to a few hundred micrometers. Their grasping motion is generated by electrostatic actuators (29), piezoelectric actuators (30), electrothermal actuators (31), or shape memory alloys (32). These microactuators have small motion ranges of a few micrometers, which can be increased by employing amplification mechanisms (30, 33). The amplification mechanisms consist of multiple links connected by either rotating joints or flexure hinges. For kinematic modeling of compliant flexures, a pseudo-rigid-body model is often used in which a flexure hinge is approximated as a rigid U joint and torsional springs (34). The pseudo-rigid-body model, however, considers only the compliance of flexures in their moving directions and cannot be used for full kinematic analysis. To analyze the kinematics of flexures, a compliance matrix with six-dimensional compliance, including tension and bending, can be used (35). More detailed information on microgrippers can be found in reviews by Yang & Xu (36) and Verotti et al. (37).

Micropipettes are standard single-ended probes that are conventionally used in life sciences and widely used in robotic micromanipulation. They are commercially available and can also be custom fabricated by laser-pulling a glass tube or a solid glass rod into a small tip with a diameter ranging from submicrometers to a few hundred micrometers. Micropipettes are usually connected to a pneumatic or hydraulic pump to control the pressure at the micropipette tip for extraction (38), translocation (39), and characterization (40) of micro-objects. Multiple micropipettes can also be cooperatively controlled for more complex manipulation tasks (41). Commercially available AFM probes are also often used in robotic micromanipulation. These probes can be used as end effectors without sensing functions, or the position of the probe and the force that the probe applies to the object being manipulated can be accurately sensed and controlled (42, 43). With modifications to standard AFM probes, specialized probes have also been developed by etching hollow channels for force-controlled micromanipulation and fluid delivery (44).

Compared with micropipettes and AFM probes, microgrippers offer more flexibility for micromanipulation. All grasping fingers can be simultaneously actuated with only one DOF, or each finger can be independently actuated with one or two DOFs (15). Microgrippers can also be integrated with position and/or force sensors, allowing the position of the gripping fingers and the grasping force to be accurately controlled in closed loop (for more details on force control, see Section 4). However, releasing a micro-object using microgrippers is more complex than using single-ended probes. To facilitate object release, additional actuators can be integrated into the microgripper to provide impact forces (45), or a liquid bridge (droplet) can be introduced between the gripping finger and the object. The thickness of the liquid bridge can be adjusted via electrowetting (46) or temperature control (47) to achieve gripping or object release.

3. FIELD-DRIVEN MICROMANIPULATION

In field-driven micromanipulation, the mechanically connected manipulator joints are replaced with components generating an actuation field, such as a magnetic, optical, acoustic, electric, or fluidic field. The end effector is not mechanically tethered to the manipulator; instead, it is

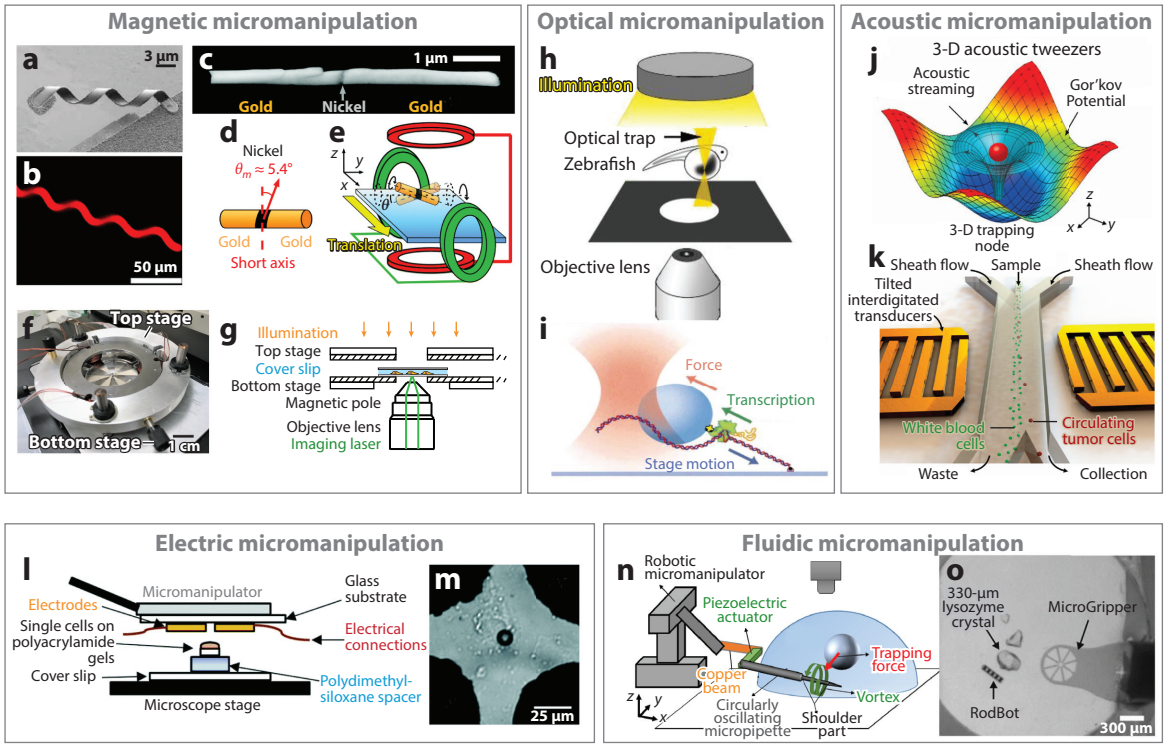

Figure 3

Field-driven micromanipulation strategies. (*Top left panels*) Magnetic micromanipulation. (*a*) Magnetic helical swimmer fabricated from self-rolled semiconductive layers. Panel adapted from Reference 59 with permission from AIP Publishing. (*b*) Fluorescence image of nanoparticles-coated *Spirulina platensis* as a biodegradable helical swimmer. Panel adapted from Reference 19 with permission from the American Association for the Advancement of Science. (*c–e*) Scanning electron microscopy image (panel *c*) and schematic (panel *d*) of a gold–nickel–gold segmented nanowire, along with the magnetic actuation of the segmented nanowire (panel *e*). Panels adapted from Reference 57 with permission from the Royal Society of Chemistry. (*f,g*) A multipole magnetic tweezer device integrated with a confocal microscope (panel *f*) and the imaging and illumination light paths (panel *g*). Panels adapted from Reference 56 with permission from IEEE. (*Top center panels*) Optical micromanipulation. (*h*) In vivo manipulation of individual biological cells inside a zebrafish using optical tweezers. Panel adapted from Reference 69 with permission from IEEE. (*i*) Schematic of an optical-tweezers-based assay for measuring the force on RNA polymerase during DNA transcription. Panel adapted from Reference 68 with permission from Cell Press. (*Top right panels*) Acoustic micromanipulation. (*j*) Acoustic field around a particle in 3-D acoustic tweezers. Panel adapted from Reference 74 with permission from the National Academy of Sciences. (*k*) Schematic illustration of an acoustic tweezer device for cell separation. Panel adapted from Reference 75 with permission from the National Academy of Sciences. (*Bottom left panels*) Electric micromanipulation. (*l*) Schematic of a microfabricated dielectrophoretic (DEP) device for particle and cell manipulation. Panel adapted from Reference 79 with permission from the Royal Society of Chemistry. (*m*) A single suspended bead trapped and manipulated inside the DEP device. Panel adapted from Reference 79 with permission from the Royal Society of Chemistry. (*Bottom right panels*) Fluidic micromanipulation. (*n*) Schematic of trapping and transportation using a fluid vortex induced by oscillation of a single piezoelectric actuator. Panel adapted from Reference 82 with permission from MDPI. (*o*) Protein crystal harvesting using fluid vortices created by a rolling microrobot. Panel adapted from Reference 83 with permission from Elsevier.

often a mobile microrobot itself [e.g., an untethered microgripper (48, 49)] or the field itself (see **Figure 3**).

3.1. Magnetic Micromanipulation

Magnetic micromanipulation, which has the advantages of untethered control and high precision, has undergone significant advances in the last decade. When a magnetic object is placed

in a magnetic field, it is subjected to a magnetic force and/or a magnetic torque. Magnetic micromanipulation can be categorized into gradient-based micromanipulation and torque-based micromanipulation.

3.1.1. Gradient-based manipulation. The magnetic force $\mathbf{F}$ exerted on a magnetic object is $\mathbf{F} = \mathbf{m}\nabla\mathbf{B}$, where $\mathbf{F}$ is the external magnetic field and $\mathbf{m}$ is the magnetic dipole moment of the object. The object with the magnetic dipole, either induced or permanent, is subject to a magnetic force when the magnetic gradient $\nabla\mathbf{B}$ exists. The magnetic gradient can be generated by electromagnetic coils or permanent magnets. Electromagnetic coils generate a controllable magnetic gradient field when an electric current is applied to them, which is then used to exert forces on the magnetic object. For example, in the multipole magnetic tweezer system (50), a controllable gradient field is generated near the pole tips. The current in each coil can be controlled in order to generate a high magnetic gradient (∼50 T/m) that can then be used to position a 5-μm magnetic bead in three dimensions. Other well-known systems utilizing electromagnetic coils, including magnetic resonance imaging (MRI)–based systems (51), OctoMag (52), and MiniMag (53), were also designed to generate a magnetic gradient in the workspace by controlling the current in each coil. Permanent magnetic systems have the advantages of low heat generation and a strong field, in which the positions and/or directions of the permanent magnets are controlled to create an inhomogeneous magnetic field flux and thus a magnetic gradient. For example, Ryan & Diller (54) designed a rotatory permanent magnet system to control the moment direction of eight permanent magnets and created a controllable magnetic gradient field of up to 2 T/m in order to position a submillimeter object in three dimensions. With gradient-generated forces, devices in the size range of centimeters to submillimeters have been actuated to perform imaging, biopsies, and surgery inside organs (e.g., the stomach, ear, and eye) (52), serve as controllable valves in microfluidic channels (55), and navigate a microdevice inside a mouse embryo for measurement (50).

However, when the object to manipulate is scaled down to microscales and below, gradient-generated forces become as small as a few piconewtons. According to the scaling law, the magnetic force scales with the magnetic moment and decreases with the third power of the object's size. Therefore, to generate a force of tens of piconewtons and greater for micromanipulation and measurement, magnetic coils (or their magnetic poles) must be placed sufficiently close to the manipulated object since the magnetic gradient scales by a factor of four with the distance between the magnetic coils and the object to manipulate. For instance, Wang et al. (56) were able to exert a force as large as 60 pN on a 0.7-μm magnetic bead in a small workspace of 40 μm × 40 μm × 20 μm to perform mechanical measurements inside a cell.

3.1.2. Torque-based manipulation. The magnetic torque $\mathbf{T}$ is exerted on the magnetic dipole as $\mathbf{T} = \mathbf{m} \times \mathbf{B}$. The magnetic torque causes a magnetic object to rotate until the direction of the dipole is aligned with the magnetic field. Through the magnetic torque, a time-variant magnetic field can rotate a magnetic object on a 2-D surface or propel a helical microswimmer in 3-D space. When magnetic torque is used to actuate a magnetic object to rotate on a 2-D surface, the object is called a surface walker or surface roller (57). These surface walkers are usually (but not always) wire-shaped objects and rotate about their short axes because of the magnetic shape anisotropy—i.e., high-aspect-ratio shapes (long rods and wires) are preferentially magnetized along the long axis. When the roller is sufficiently heavy and rolls on the surface, the friction between the roller and the surface moves the object forward. For example, a dumbbell surface walker was made by assembling a nickel nanowire to two polymer microbeads; through the application of rotating magnetic fields, the walker generated vortices that were used for micro-object transportation (58).

Magnetic torque has also been used to propel helical magnetic objects in 3-D. Inspired by the bacterial flagellum, Zhang et al. (59) designed and fabricated a helical magnetic microswimmer (**Figure 3*a***). The helical microrobot has a magnetic head and a helical tail that rotates around its helical axis under a rotating magnetic field to move forward or backward in the direction perpendicular to the plane of rotation. As the torque depends on the magnitude of the magnetic flux density **B** (in contrast to a force that depends on the gradient of **B**), the torque is easier to generate by a strong magnetic field, for example, using Helmholtz coils. Due to the large output of torque generation and its convenience of application to swarm control using a large magnetic flux density, the helical microswimmers actuated by rotatory magnetic fields have shown great promise in drug delivery (60), gene delivery (61), and cell delivery (62). Loaded with stimulus-responsive agents (e.g., liposomes or bacteria), these microrobots can perform smart delivery in response to pH or temperature changes (18). Yan et al. (19) navigated a swarm of helical swimmers, constructed by coating magnetic nanoparticles onto the surface of helical-shaped biodegradable *Spirulina platensis*, in the peritoneal cavity of a mouse.

The magnetic gradient and torque can also be used together for micromanipulation. The magnetic gradient, which generates controllable but limited forces, can be used to position a magnetic object for locomotion, while magnetic torque can be exerted on the object to rotate it or induce shape changes for actuation or grasping. For example, Zhang et al. (63) assembled multipole microscale bricks with different magnetic moment directions to form a base–arm–finger structure for grasping micro-objects. They used a magnetic gradient to navigate the assembled device close to a target, then used magnetic torque to induce conformational shape changes in the structure to generate a grasping motion.

3.2. Optical Micromanipulation

Optical micromanipulation has been applied to many areas, including microassembly, biophysical characterization, and cell manipulation. It utilizes the optical field created by focused laser beams. When laser beams create a highly focused optical field near the object being manipulated (e.g., a microparticle), gradient force and scattering force are generated. The gradient force stems from the intensity gradient of the electric field of the focused laser beams, and the scattering force results from the optical momentum of the light transferred to the particle. The balance between these two forces results in an equilibrium point near the focus location. Optical micromanipulation uses visual feedback to control the position of the equilibrium point and manipulate trapped objects in 3-D. Arai et al. (64) developed synchronized optical micromanipulation strategies in which the laser scanning patterns of a single laser are varied to control multiple targets independently.

Based on visual servoing and optical tweezers' ability to rapidly generate high-resolution forces (at the piconewton level), robotic optical micromanipulation has been applied to sort and transport cells (**Figure 3*b***). The target cells, including yeast cells (65), live sperm cells (66), and embryonic stem cells (67), are trapped by the optical field and manipulated to designated locations. The force generated by laser tweezers is typically on the scale of piconewtons. While such forces are large enough to sort and transport cells and molecules (68) (**Figure 3*i***), they are limited for applications such as cell mechanics and tissue engineering, where nanonewton forces are often required for mechanical measurement or stimulation. Increasing the laser power can further increase the force but can also damage the object being manipulated.

Considering the low force output, Brownian motion and thermal disturbances pose challenges to robotic optical micromanipulation. Significant efforts have been made to develop control, tracking, and planning methods for high-precision sorting and transportation of micro-objects. For instance, a disturbance compensation controller (69), stochastic path planning (70), and modified

A* path planning (71) were developed for transporting cells inside tissue to compensate for force disturbances caused by Brownian motion and blood flow.

3.3. Acoustic Micromanipulation

Acoustic micromanipulation, which is a dynamic and noninvasive technique, manipulates a specimen using sound waves. Interdigital transducers deposited on a piezoelectric substrate convert electric signals to surface acoustic waves by generating periodically distributed mechanical forces. The objects being manipulated are pushed to either acoustic pressure nodes (minimum-pressure regions) or pressure antinodes (maximum-pressure regions), depending on the density and compressibility of the object, as shown in **Figure 3*j***. Micromanipulation of objects using sound waves is achieved by controlling the positions of pressure nodes (72).

Acoustic waves or acoustic tweezers have been used to trap and manipulate microscale particles and biological cells without direct contact, which has important applications in biology, chemistry, engineering, and medicine (73). Piezoelectric transducers are often integrated into microfluidic devices for high-throughput cell sorting and assembly, as shown in **Figure 3*j*** (74). Viruses and circulating tumor cells have also been purified from blood using acoustic tweezers for diagnostic applications, as shown in **Figure 3*k*** (75), and cells have been assembled using acoustic tweezers inside a microfluidic chip to create engineered tissues (76). Compared with optical tweezers and magnetic tweezers, which generate a local field to manipulate a single object, acoustic tweezers are advantageous in swarm control because the acoustic wave has multiple pressure nodes to trap the objects to manipulate. Additionally, acoustic tweezers have a large force output (e.g., 150 pN on particles smaller than 5 μm) compared with magnetic tweezers and optical tweezers (which typically generate forces of approximately 50 pN and 10 pN, respectively, on a particle of the same size) (77). To manipulate submicrometer objects, the acoustic waves generated by integrated transducers must have a wavelength comparable to the size of the objects.

3.4. Electric Micromanipulation

Microparticles suspended in fluids respond to AC and DC electric fields through several mechanisms. When a DC field is applied to polarizable particles, the charged particles move toward oppositely charged electrodes by electrophoresis. When an AC field is applied, the electric field exerts a dielectrophoretic force on the particles. Particles of a few nanometers to tens of micrometers can be manipulated by controlling the field strength, frequency, and electrode geometries. In addition to direct electric force applied to the micro- and nanoparticles, DC or AC electrokinetics may drive liquid flows inside the workspace and further lead to the transportation and redistribution of the suspended particles. Electric micromanipulation, through either an AC or DC electric field, has been used for microassembly of nanoparticles and nanowires (78), measurement of single-cell mechanics (**Figure 3*l***), microbead manipulation (79) (**Figure 3*m***), and DNA analysis (80). However, the electric force applied to the manipulated targets strongly depends on the electrical properties of the medium and the size, shape, and electrical properties of the target particles (79). Recent advances in optical dielectrophoresis synergistically leverage both optical and electric fields and use a light intensity approximately 1,000 times less than that of traditional optical tweezers for programmable and less invasive micromanipulation (81).

3.5. Fluidic Micromanipulation

For fluidic micromanipulation, a fluidic field can be generated by oscillating piezoelectric actuators, rotating a magnetic rod-shaped microrobot, or controlling the flow rate inside a micropipette.

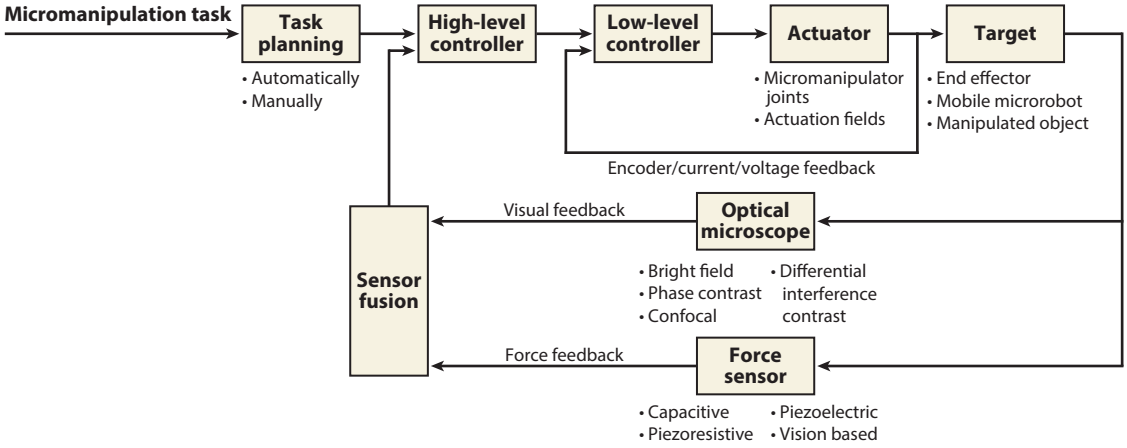

Figure 4

Control architecture in robotic micromanipulation, in which the micromanipulation task is either automatically planned with a task planner or manually planned with human input. A high-level controller receives visual and/or force feedback and computes the desired input for the actuator (e.g., desired motor velocity or desired current for magnetic micromanipulation). A low-level controller receives sensor feedback from the actuator (e.g., encoder position feedback) and controls the actuator to follow the desired input.

For instance, fluid vortices were created by oscillating a micropipette connected to a piezoelectric actuator to trap and transport 100-μm beads (**Figure 3*n***) (82), a rod-shaped microrobot was controlled by using a rotating magnetic field and visual servoing to generate vortices to manipulate protein crystals (**Figure 3*o***) (83), and fluidic flow was controlled in a micropipette for rotating (84), transporting, and depositing (85) biological cells. Quantifying and controlling the fluidic force exerted on the target object during manipulation can be challenging due to the difficulty of accurately modeling fluid dynamics.

4. CONTROL

Vision, force, and position are the most common modalities of feedback in robotic micromanipulation. **Figure 4** shows a general control diagram; this section discusses how visual and force feedback is obtained in robotic micromanipulation and how the high-level controller in this architecture is designed.

4.1. Visual Servoing

Optical microscopes provide high-resolution (up to ∼0.2 μm), small-field-of-view (smaller than a few square millimeters), and low-depth-of-field (less than tens of micrometers) visual feedback. Visual servoing with computer vision microscopy feedback aims to minimize the error between the features $\mathbf{s}(t)$ extracted from microscopy images and the desired features $\mathbf{s}^*$. The typical features $\mathbf{s}(t)$ are the image coordinates of the centroid of the servoed object, which can be an end effector, a mobile microrobot, or an object to manipulate. The classical proportional controller (86) assumes an exponential decrease of the error, $\mathbf{v} = -\lambda \mathbf{L}_s^+[\mathbf{s}(t) - \mathbf{s}^*]$, where $\mathbf{v}$ is the controller output, λ is the controller gain, and $\mathbf{L}_s^+$ is the pseudoinverse of the interaction matrix $\mathbf{L}_s$ (also called the image Jacobian matrix). $\mathbf{L}_s$ relates the velocity of the servoed object in the global Cartesian space to the velocity of the same object in the image space.

With the camera fixed on the microscope, visual servoing under microscopes almost always uses an eye-to-hand configuration. In this configuration, the controller output $\mathbf{v}$ is the velocity

of the servoed object with respect to the camera's coordinate frame. For visual servoing of a motorized micromanipulator, the controller output **v** is a set of velocities of the manipulator joints that directly change the velocity of the end effector. For field-driven micromanipulation without manipulator joints, the velocity of the microrobot or manipulated object is indirectly adjusted by changing the current or voltage that controls the field. Hence, the controller should additionally include the dynamics model that correlates the velocity of the microrobot or the manipulated object with the current or voltage controlling the field (50, 87).

The magnifications of a microscope require modifications to the interaction matrix $\mathbf{L}_s$. A zoom factor, defined as the ratio between the objective lens's focal length and the tube lens's focal length, can be added to the interaction matrix (88). Alternatively, the focal lengths of the objective lens and the tube lens can be added as two additional dimensions to the interaction matrix (89). The limited depth of field of a microscope only allows viewing a single plane perpendicular to the optical axis. Attention needs to be paid to avoid choosing coplanar image features, as they may cause singularities in the interaction matrix (90). To calibrate the interaction matrix, Zhou & Nelson (91) fabricated planar calibration patterns on a glass slide and applied iterative single-plane calibration methods, using parameters (e.g., focal length) provided by microscope manufacturers as initial values. Ammi et al. (92) generated virtual calibration patterns by using a micromanipulator to move an end effector tip in 3-D space. They estimated the interaction matrix using the 3-D coordinates obtained from the micromanipulator.

The microscope imaging mode must also be considered when obtaining visual feedback $\mathbf{s}(t)$. For bright-field images, general computer vision algorithms can be readily used for noise reduction, image segmentation, feature extraction, and target tracking. Contrast imaging modes, such as phase-contrast microscopy and differential interference contrast microscopy, use polarized light illumination to convert the difference in optical path lengths into image intensity to enhance contrast but also cause halo or side illumination effects (93). These effects lead to inhomogeneous image intensity, which must be accounted for before image segmentation algorithms can be applied. For instance, the Hilbert algorithm transforms an image into the frequency domain and reverses the sign of the components with negative frequencies to remove the inhomogeneity in image intensity (94). The Wiener filtering algorithm can also be applied to deconvolute the image with the point-spread function (i.e., the spatial domain version of the optical transfer function) of the contrast imaging modes (95).

To obtain depth information along the z axis, confocal microscopy can be used to scan images along the z axis to provide image stacks, or a second microscope can be added for imaging from the side (96, 97). Micromanipulation under confocal microscopes, however, requires fluorescently labeling both the end effector or microrobot and the manipulated object for clear visualization (56, 98). Laser scanning confocal microscopes usually have a low bandwidth (e.g., less than 10 frames per second). A higher bandwidth of a few hundred frames per second can be obtained using spinning-disk confocal microscopes, but with the sacrifice of worse imaging resolution along the z axis and higher background noise than those obtained by laser scanning confocal microscopes (99).

Regular microscopy vision feedback can also be used during micromanipulation to estimate depth information. For example, when an end effector is lowered along the z axis, once the contact between the end-effector tip and the substrate or manipulated object is established, the contact can be visually detected based on the change in the motion of the end-effector tip (100) or the deformation of the contacted object (101). This vision-based contact detection method can achieve an accuracy of 0.2 μm but requires multiple frames of images to accurately determine a reference z coordinate of the substrate or the manipulated object (100). Once the reference

z coordinate is set, the depth can be obtained in real time by subtracting it from the current z coordinate of the micromanipulator.

Vision algorithms have also been developed to directly calculate depth information from microscopy images. Most of these algorithms use the focus–defocus method to estimate the relative z coordinate between the current focal plane and a reference plane (102), with images of the manipulated object or end effector at different focal planes stored as a reference library (103). The position and pose of the end effector can also be estimated when a priori knowledge [e.g., the computer-aided design (CAD) model of an object] is available (104, 105). In general, focus–defocus approaches are sensitive to the microscope's illumination conditions and the focus algorithm selection. The resolution of focus–defocus approaches is limited by the axial resolution (i.e., the depth of field) of the microscope. For instance, using a 20× objective lens with a typical numerical aperture of 0.4, two objects with a z coordinate difference of 5.8 μm are both in focus in images and cannot be differentiated.

Besides the classical proportional controller, more sophisticated controllers have also been developed for different robotic micromanipulation tasks. For the visual servoing of a moving object, Zhang et al. (106) added a feedforward compensator in the high-level controller (**Figure 4**) to compensate for the movement of the object. Leung et al. (84) developed controllers to switch between in-plane (x–y axes) control and out-of-plane (z axis) control. To position multiple objects in a micropipette using fluidic fields, Zhang et al. (85) developed an optimal controller to minimize the volume of the excess medium aspirated together with the object. For simultaneous visual servoing of multiple magnetic objects, Diller et al. (107) modeled the dynamics, including the interaction between multiple magnetic objects, and integrated them into the controller.

4.2. Force Sensing and Control

For closed-loop force-controlled micromanipulation (**Figure 4**), force sensors are integrated into the micromanipulator, end effector, or mobile microrobots. In robotic micromanipulation, force sensors are used to measure forces typically at the level of micronewtons and below. Several microforce sensors based on capacitive, piezoresistive, and piezoelectric principles have been developed (108). Compared with macroscale force sensors, which can be easily mounted to a robotic arm, it is more difficult to integrate microforce sensors into a micromanipulator, end effector, or microrobot. For example, piezoresistive or piezoelectric microforce sensors must be carefully mounted (e.g., glued), to predefined positions along proper orientations in the micromanipulation system (108). When the mechanical properties of a microstructure are known, vision can be used to estimate force information. Jing & Cappelleri (109) integrated a microbeam with calibrated low stiffness (0.01 N/m) into a magnetic microrobot and calculated the force applied by the microrobot by visually measuring the deformation of the microbeam.

In most field-driven micromanipulation, however, it is difficult to integrate force sensors into the mobile microrobot. Instead, the relationship between the applied force and the current or voltage used to control the field can be theoretically calculated and experimentally calibrated (50, 110). For instance, in gradient-based magnetic micromanipulation, the force exerted on the microrobot can be calculated by using its dipole moment $\mathbf{m}$ and the gradient of the external magnetic field ($\nabla\mathbf{B}$). In optical micromanipulation, there are at least two models for force prediction depending on the size of the trapped particle and the wavelength of the trapping light. For objects that are significantly smaller than the wavelength of light, the conditions for Rayleigh scattering are satisfied, and the particle can be manipulated as a point dipole in an inhomogeneous electromagnetic field. Accordingly, the force applied to the trapped particle is calculated as the Lorentz force. For objects that are much larger than the laser's wavelength [e.g., biological cells of tens of micrometers

compared with a neodymium-doped yttrium aluminum garnet (Nd:YAG) laser with wavelength of 1,064 nm], the force can be calculated with the ray-optics model (87). In a simplified model for cell manipulation with optical tweezers, the trapping force is often considered proportional to the distance between the cell and the laser when the cell is close to the laser beam (110).

One common goal of closed-loop force control in micromanipulation is to reduce the impact force at the tip of a probe or to control the force applied to the manipulated object. In impact-force control, one typical solution is to design a hybrid controller that seamlessly switches between position control and force control, with feedback from position sensors (e.g., encoders) and microforce sensors (111). The hybrid control system first controls the speed and position of a micromanipulator until the end effector is close to the target object, which can be identified by visually detecting the presence and motion of the end effector in the microscope's field of view, and then switches to force control until the desired impact force is achieved. This switching control approach has been demonstrated to be effective for controlling the impact force and protecting the fragile end effector and target object in micromanipulation (112). To control the microforce applied to the target object, the system characteristics need to be analyzed and integrated in the force controller. For example, Dario (113) obtained the frequency response for both the idle (i.e., not grasping) and grasping phases for force-controlled micromanipulation. In robotic cell manipulation, force–position relationships derived from cell mechanics can be used to control the out-of-plane position of the end effectors by utilizing an impedance controller to maintain the manipulation force at a desired level (114).

Force control is also crucial for providing haptic feedback in teleoperated micromanipulation, where a master human–robot interface is used to operate a slave microrobot. In the master–slave system architecture, the critical problem is to properly scale the positions from the master end to the microscale and scale up the contact forces in the microworld to provide feedback to the operator. Ideally, the teleoperated system should provide a geometric similarity and dynamic similarity, and the operator should be able to control the slave robot with minimal distortion of information. One method to achieve this goal is to use an impedance controller to remodel the microscale environment (115). A limitation of impedance control is that the force feedback to the master is calculated from the velocity and acceleration with a simple mass-spring model of the slave system. The simplified dynamic models may not be accurate since the dominating forces (e.g., van der Waals forces and capillary forces) at the microscale are complex and nonlinear. In teleoperation with optical tweezers, forces are often measured by high-speed video cameras and then scaled up from the piconewton level to the newton level in order to provide a sensation through the haptic interface (116).

5. SUMMARY AND OUTLOOK

Table 1 summarizes major milestones in robotic micromanipulation in chronological order. The use of robotic micromanipulation for microassembly dates back to the 1990s. Fatikow et al. (117) and Yang et al. (118) used robotic microassembly for the 3-D integration of heterogeneous components to construct miniaturized devices. Since serial assembly via robotic pick and place suffered from low assembly efficiency, and most micromanipulation systems were developed for a specific task and lacked the versatility to assemble disparate micro-objects, parallel microassembly was developed for increased throughput. Adhesion-based transfer printing using an elastomer stamp enabled the assembly of diverse materials, such as silicon and graphene, with a throughput of millions of objects per hour (119). Parallel arrays of nanowires and carbon nanotubes were deterministically positioned to construct sensors and transistors (120). The integration of transfer printing with robotics has potential for parallel assembly with high efficiency and accuracy.

Another parallel microassembly approach is to use micromachined cavities, electrostatic traps, or capillary force for self-assembly (121). Capillary-force-driven self-assembly was developed for the assembly of piezoelectric actuators and for self-transport and self-alignment of microchips (122). A swarm of microrobots has also been magnetically controlled for programmable 3-D assembly of microparts (48, 123). To control the microrobots individually for distributed operation, different magnetic forces were exerted on each geometrically or magnetically distinct microrobot. Control strategies for autonomous planning and cooperative assembly are necessary to unleash the full potential of multiple microrobots. Besides microassembly for device construction, 3-D cellular structures have been assembled for tissue engineering applications. For instance, vasculature-like microtubes were robotically assembled for nutrient delivery (124), and cell-encapsulating hydrogels were assembled into biological constructs by untethered magnetic microrobots (125, 126).

Since the early 2000s, robotic micromanipulation techniques have been developed for manipulating biological cells (8). Mechanical characterization of single cells has been enabled by microforce sensors (127, 128) and force-feedback microgrippers (129). Several control strategies were developed to accurately position micropipettes and control force interactions with cells during cell manipulation, including switching impedance control (130), sliding mode control (131), and adaptive control (132). Around 2010, robotic intracytoplasmic sperm injection was invented for clinical in vitro fertilization (16), representing the first effort to pursue clinical robotic surgery at the cellular level (i.e., robotic cell surgery). Robotic cell manipulation techniques were also developed for manipulating adherent cells (133, 134). A robotic adherent cell manipulation system was created for measuring cell–cell communication on large-scale samples (thousands of cells versus tens of cells in manual operation) with a success rate higher than 95% (26). The technology was used for testing drug efficacy in pursuit of cardiac arrhythmia treatment (135).

More recently, the era of robotic intracellular manipulation and measurement began. The ability to directly interrogate intracellular structures inside a single cell for measurement and manipulation has significant implications for understanding subcellular and suborganelle activities, diagnosing diseases, and developing new therapeutic approaches (136). Wang et al. (56) three-dimensionally positioned a submicrometer magnetic bead in a cell using a generalized predictive controller. The system was also capable of three-dimensionally applying a force of up to 60 pN with a resolution of 4 pN. The submicrometer bead was magnetically controlled to move from an initial position in a cell to multiple target positions on the cell nucleus. The results revealed that significantly higher stiffness exists in the major axis of a cell nucleus than in its minor axis, and the cell nucleus stiffens upon the application of an intracellularly applied force (56).

Field-driven micromanipulation has significantly developed over the past decade, employing magnetic, optical, acoustic, electric, fluidic, and other fields. Among these techniques, magnetic micromanipulation has the advantages of specificity, large force output, and deep tissue penetration. At the organ level, magnetically actuated microrobots have been controlled inside the eye for untethered surgery and drug delivery (137), and magnetic capsule endoscopes and magnetically guided catheters have been developed for intraorgan imaging and/or biopsy (138, 139). At the tissue level, microassembly of tissue constructs was achieved via magnetic micromanipulation (126), and magnetically controlled microtransporters have delivered cells to target sites for cell therapies (140). At the cell level, magnetic beads have been controlled by external magnetic fields to probe the inside of a single embryo (50) or a single cell (56) for stimulation and characterization. Due to the poor scaling of magnetic force, magnetic microrobots can lack sufficient propelling forces for navigation in vivo. Thus, biohybrid magnetic microrobots utilizing self-propelled bacteria were developed and successfully delivered drugs deep into the hypoxic region of a tumor (18). These swarms of bacteria consisted of *Magnetococcus marinus* bacterial strain MC-1 containing magnetosomes that respond to external magnetic fields, but other magneto-bacteria can also be

used to form biohybrid magnetic microrobots (141). In the pursuit of clinical deployment, shear from the bloodstream, immune responses (e.g., effects from macrophages), and the mechanical inhomogeneity of different types of tissues or organs require more robust propulsion, sensing, and control. The safety requirements for in vivo applications also demand that untethered magnetic microrobots be traceable, biocompatible, and retractable or biodegradable. Therefore, biodegradable materials, such as degradable hydrogel composites (60), biohybrid microswimmers (142), and biological matrices (19), have become a focus in recent studies of magnetically actuated microrobots.

For closed-loop in vivo navigation of untethered microrobots, visual servoing with image feedback from clinical imaging systems such as MRI, computed tomography (CT), and ultrasound is also under intensive development. Presently, commercial MRI and CT systems have a typical spatial resolution of 200–500 μm and a bandwidth of less than a few frames per second (143, 144). A higher bandwidth of 30 frames per second can be achieved by using real-time MRI, but with the trade-off of poorer spatial resolution of approximately 1.5 mm (145). Ultrasound imaging can achieve up to 100 frames per second and a high spatial resolution of a few micrometers by using high-frequency sound waves [e.g., >100 MHz (146)]; however, its low signal-to-noise ratio (e.g., structures such as bones that strongly reflect sound waves can cause artifacts in ultrasound imaging) poses difficulties in robust image processing. The rapid advances of clinical imaging technologies, such as ultrasound elastography (147) and photoacoustic tomography (148), will play an integral role in the eventual clinical applications of untethered mobile microrobots.

As one can see from the summary in **Table 1**, robotic micromanipulation is a relatively young field. However, fundamental physics; techniques for sensing, actuation, and control; tool sets and systems; and, more importantly, a research community are now in place after three decades of development and evolution. On the one hand, there is still plenty of room for innovation, such as image-guided navigation and control in the in vivo environment and the development of new robotic micromanipulation techniques using acoustic fields. On the other hand, the next few years will likely witness a more tangible impact of robotic micromanipulation in industry and clinical settings. The endless creativity and passion instilled by the robotic micromanipulation community will continue, and this vibrant field will undergo more exciting and transformative development over the next decade.

DISCLOSURE STATEMENT

The authors are not aware of any affiliations, memberships, funding, or financial holdings that might be perceived as affecting the objectivity of this review.

ACKNOWLEDGMENTS

The authors acknowledge support from the Natural Sciences and Engineering Research Council of Canada (NSERC), the Canadian Institutes of Health Research (CIHR), the Canada Research Chairs Program, Mitacs, Ontario Centres of Excellence (OCE), and Ontario Research Funds (ORF).

LITERATURE CITED

1. Fukuda T, Fujiyoshi M, Arai F, Matsuura H. 1991. Design and dextrous control of micromanipulator with 6 DOF. In *Proceedings of the 1991 IEEE International Conference on Robotics and Automation*, pp. 1628–33. New York: IEEE

2. Arai F, Ando D, Fukuda T, Nonoda Y, Oota T. 1995. Micro manipulation based on micro physics-strategy based on attractive force reduction and stress measurement. In *Proceedings of the 1995 IEEE/RSJ International Conference on Intelligent Robots and Systems: Human Robot Interaction and Cooperative Robots*, Vol. 2, pp. 236–41. New York: IEEE
3. Fearing RS. 1995. Survey of sticking effects for micro parts handling. In *Proceedings of the 1995 IEEE/RSJ International Conference on Intelligent Robots and Systems: Human Robot Interaction and Cooperative Robots*, Vol. 2, pp. 212–17. New York: IEEE
4. Rembold U, Fatikow S. 1997. Autonomous microrobots. *J. Intell. Robot. Syst.* 19:375–91
5. Kallio P, Zhou Q, Koivo HN. 1998. Control issues in micromanipulation. In *Proceedings of the 1998 International Symposium on Micromechatronics and Human Science*, pp. 135–41. New York: IEEE
6. Nelson BJ, Zhou Y, Vikramaditya B. 1998. Sensor-based microassembly of hybrid MEMS devices. *IEEE Control Syst.* 18:35–45
7. Bohringer K-F, Donald BR, MacDonald NC. 1999. Programmable force fields for distributed manipulation, with applications to MEMS actuator arrays and vibratory parts feeders. *Int. J. Robot. Res.* 18:168–200
8. Sun Y, Nelson BJ. 2002. Biological cell injection using an autonomous microrobotic system. *Int. J. Robot. Res.* 21:861–68
9. Dreyfus R, Baudry J, Roper ML, Fermigier M, Stone HA, Bibette J. 2005. Microscopic artificial swimmers. *Nature* 437:862–65
10. Donald BR, Levey CG, McGray CG, Paprotny I, Rus D. 2006. An untethered, electrostatic, globally controllable MEMS micro-robot. *J. Microelectromech. Syst.* 15:1–15
11. Yesin KB, Vollmers K, Nelson BJ. 2006. Modeling and control of untethered biomicrorobots in a fluidic environment using electromagnetic fields. *Int. J. Robot. Res.* 25:527–36
12. Ghosh A, Fischer P, Ghost A, Fischer P. 2009. Controlled propulsion of artificial magnetic nanostructured propellers. *Nano Lett.* 9:7–9
13. Martel S, Tremblay CC, Ngakeng S, Langlois G. 2006. Controlled manipulation and actuation of micro-objects with magnetotactic bacteria. *Appl. Phys. Lett.* 89:233904
14. Magdanz V, Sanchez S, Schmidt OG. 2013. Development of a sperm-flagella driven micro-bio-robot. *Adv. Mater.* 25:6581–88
15. Agnus J, Chaillet N, Clévy C, Dembélé S, Gauthier M, et al. 2013. Robotic microassembly and micromanipulation at FEMTO-ST. *J. Micro-Bio Robot.* 8:91–106
16. Lu Z, Zhang X, Leung C, Esfandiari N, Casper RF, Sun Y. 2011. Robotic ICSI (intracytoplasmic sperm injection). *IEEE Trans. Biomed. Eng.* 58:2102–8
17. Sitti M, Ceylan H, Hu W, Giltinan J, Turan M, et al. 2015. Biomedical applications of untethered mobile milli/microrobots. *Proc. IEEE* 103:205–24
18. Felfoul O, Mohammadi M, Taherkhani S, De Lanauze D, Zhong Xu Y, et al. 2016. Magneto-aerotactic bacteria deliver drug-containing nanoliposomes to tumour hypoxic regions. *Nat. Nanotechnol.* 11:941–47
19. Yan X, Zhou Q, Vincent M, Deng Y, Yu J, et al. 2017. Multifunctional biohybrid magnetite microrobots for imaging-guided therapy. *Sci. Robot.* 2:eaaq1155
20. Li J, Esteban-Fernández de Ávila B, Gao W, Zhang L, Wang J. 2017. Micro/nanorobots for biomedicine: delivery, surgery, sensing, and detoxification. *Sci. Robot.* 2:eaam6431
21. Abbott JJ, Nagy Z, Beyeler F, Nelson BJ. 2007. Robotics in the small, part I: microbotics. *IEEE Robot. Autom. Mag.* 14:92–103
22. Diller E, Sitti M. 2011. Micro-scale mobile robotics. *Found. Trends Robot.* 2:143–259
23. Dong L, Nelson BJ. 2007. Robotics in the small, part II: nanorobotics. *IEEE Robot. Autom. Mag.* 14:111–21
24. Shi C, Luu DK, Yang Q, Liu J, Chen J, et al. 2016. Recent advances in nanorobotic manipulation inside scanning electron microscopes. *Microsyst. Nanoeng.* 2:16024
25. Li M, Dang D, Xi N, Wang Y, Liu L. 2018. A review of nanoscale characterizing individual DNA behaviors using atomic force microscopy. *IEEE Trans. Nanotechnol.* 17:920–33

26. Liu J, Siragam V, Gong Z, Chen J, Fridman MD, et al. 2015. Robotic adherent cell injection for characterizing cell-cell communication. *IEEE Trans. Biomed. Eng.* 62:119–25
27. Kodandaramaiah SB, Flores FJ, Holst GL, Singer AC, Han X, et al. 2018. Multi-neuron intracellular recording in vivo via interacting autopatching robots. *eLife* 7:e24656
28. Das AN, Murthy R, Popa DO, Stephanou HE. 2012. A multiscale assembly and packaging system for manufacturing of complex micro-nano devices. *IEEE Trans. Autom. Sci. Eng.* 9:160–70
29. Xu Q. 2015. Design, fabrication, and testing of an MEMS microgripper with dual-axis force sensor. *IEEE Sens. J.* 15:6017–26
30. Wang F, Liang C, Tian Y, Zhao X, Zhang D. 2016. Design and control of a compliant microgripper with a large amplification ratio for high-speed micro manipulation. *IEEE/ASME Trans. Mechatron.* 21:1262–71
31. Zeman MJF, Bordatchev EV, Knopf GK. 2006. Design, kinematic modeling and performance testing of an electro-thermally driven microgripper for micromanipulation applications. *J. Micromech. Microeng.* 16:1540
32. Nikdel N, Nikdel P, Badamchizadeh MA, Hassanzadeh I. 2014. Using neural network model predictive control for controlling shape memory alloy-based manipulator. *IEEE Trans. Ind. Electron.* 61:1394–401
33. Xu Q, Li Y. 2011. Analytical modeling, optimization and testing of a compound bridge-type compliant displacement amplifier. *Mech. Mach. Theory.* 46:183–200
34. Yun Y, Li Y. 2011. Optimal design of a 3-PUPU parallel robot with compliant hinges for micromanipulation in a cubic workspace. *Robot. Comput. Integr. Manuf.* 27:977–85
35. Li Y, Xu Q. 2009. Design and analysis of a totally decoupled flexure-based XY parallel micromanipulator. *IEEE Trans. Robot.* 25:645–57
36. Yang S, Xu Q. 2017. A review on actuation and sensing techniques for MEMS-based microgrippers. *J. Micro-Bio Robot.* 13:1–14
37. Verotti M, Dochshanov A, Belfiore NP. 2017. A comprehensive survey on microgrippers design: mechanical structure. *J. Mech. Des.* 139:60801–26
38. Zhang XP, Leung C, Lu Z, Esfandiari N, Casper RF, Sun Y. 2012. Controlled aspiration and positioning of biological cells in a micropipette. *IEEE Trans. Biomed. Eng.* 59:1032–40
39. Anis YH, Holl MR, Meldrum DR. 2010. Automated selection and placement of single cells using vision-based feedback control. *IEEE Trans. Autom. Sci. Eng.* 7:598–606
40. Shojaei-Baghini E, Zheng Y, Sun Y. 2013. Automated micropipette aspiration of single cells. *Ann. Biomed. Eng.* 41:1208–16
41. Wang Z, Latt WT, Tan SYM, Ang WT. 2015. Visual servoed three-dimensional cell rotation system. *IEEE Trans. Biomed. Eng.* 62:2498–507
42. Xie H, Régnier S. 2011. Development of a flexible robotic system for multiscale applications of micro/nanoscale manipulation and assembly. *IEEE/ASME Trans. Mechatron.* 16:266–76
43. Xie H, Zhang H, Song J, Meng X, Wen Y, Sun L. 2018. High-precision automated micromanipulation and adhesive microbonding with cantilevered micropipette probes in dynamic probing mode. *IEEE/ASME Trans. Mechatron.* 23:1425–35
44. Guillaume-Gentil O, Potthoff E, Ossola D, Franz CM, Zambelli T, Vorholt JA. 2014. Force-controlled manipulation of single cells: from AFM to FluidFM. *Trends Biotechnol.* 32:381–88
45. Chen BK, Zhang Y, Sun Y. 2009. Active release of microobjects using a MEMS microgripper to overcome adhesion forces. *J. Microelectromech. Syst.* 18:652–59
46. Vasudev A, Jagtiani A, Du L, Zhe J. 2009. A low-voltage droplet microgripper for micro-object manipulation. *J. Micromech. Microeng.* 19:075005
47. Fan Z, Rong W, Wang L, Sun L. 2015. A single-probe capillary microgripper induced by dropwise condensation and inertial release. *J. Micromech. Microeng.* 25:115011
48. Eric D, Metin S. 2014. Three-dimensional programmable assembly by untethered magnetic robotic micro-grippers. *Adv. Funct. Mater.* 24:4397–404
49. Ghosh A, Yoon C, Ongaro F, Scheggi S, Selaru FM, et al. 2017. Stimuli-responsive soft untethered grippers for drug delivery and robotic surgery. *Front. Mech. Eng.* 3:7

50. Wang X, Luo M, Wu H, Zhang Z, Liu J, et al. 2018. A three-dimensional magnetic tweezer system for intraembryonic navigation and measurement. *IEEE Trans. Robot.* 34:240–47
51. Vonthron M, Lalande V, Bringout G, Tremblay C, Martel S. 2011. A MRI-based integrated platform for the navigation of microdevices and microrobots. In *2011 IEEE/RSJ International Conference on Intelligent Robots and Systems*, pp. 1285–90. New York: IEEE
52. Kummer MP, Abbott JJ, Kratochvil BE, Borer R, Sengul A, Nelson BJ. 2010. OctoMag: an electromagnetic system for 5-DOF wireless micromanipulation. *IEEE Trans. Robot.* 26:1006–17
53. Schuerle S, Erni S, Flink M, Kratochvil BE, Nelson BJ. 2013. Three-dimensional magnetic manipulation of micro- and nanostructures for applications in life sciences. *IEEE Trans. Magn.* 49:321–30
54. Ryan P, Diller E. 2017. Magnetic actuation for full dexterity microrobotic control using rotating permanent magnets. *IEEE Trans. Robot.* 33:1398–409
55. Zhang J, Onaizah O, Sadri A, Diller E. 2017. A generic label-free microfluidic microobject sorter using a magnetic elastic diverter. *Biomed. Microdevices* 19:43
56. Wang X, Luo M, Ho C, Zhang Z, Zhao Q, et al. 2018. Robotic intracellular manipulation: 3D navigation and measurement inside a single cell. In *2018 IEEE International Conference on Robotics and Automation*, pp. 2716–21. New York: IEEE
57. Mair LO, Evans BA, Nacev A, Stepanov PY, Hilaman R, et al. 2017. Magnetic microkayaks: propulsion of microrods precessing near a surface by kilohertz frequency, rotating magnetic fields. *Nanoscale* 9:3375–81
58. Chen XZ, Jang B, Ahmed D, Hu C, De Marco C, et al. 2018. Small-scale machines driven by external power sources. *Adv. Mater.* 30:1705061
59. Zhang L, Abbott JJ, Dong L, Kratochvil BE, Bell D, Nelson BJ. 2009. Artificial bacterial flagella: fabrication and magnetic control. *Appl. Phys. Lett.* 94:064107
60. Peters C, Hoop M, Pané S, Nelson BJ, Hierold C. 2016. Degradable magnetic composites for minimally invasive interventions: device fabrication, targeted drug delivery, and cytotoxicity tests. *Adv. Mater.* 28:533–38
61. Qiu F, Fujita S, Mhanna R, Zhang L, Simona BR, Nelson BJ. 2015. Magnetic helical microswimmers functionalized with lipoplexes for targeted gene delivery. *Adv. Funct. Mater.* 25:1666–71
62. Wang B, Chan KF, Yu J, Wang Q, Yang L, et al. 2018. Reconfigurable swarms of ferromagnetic colloids for enhanced local hyperthermia. *Adv. Funct. Mater.* 28:1705701
63. Zhang J, Onaizah O, Middleton K, You L, Diller E. 2017. Reliable grasping of three-dimensional untethered mobile magnetic microgripper for autonomous pick-and-place. *IEEE Robot. Autom. Lett.* 2:835–40
64. Arai F, Yoshikawa K, Sakami T, Fukuda T. 2004. Synchronized laser micromanipulation of multiple targets along each trajectory by single laser. *Appl. Phys. Lett.* 85:4301–3
65. Alam MK, Koomsoon E, Zou H, Yi C, Li C-W, et al. 2018. Recent advances in microfluidic technology for manipulation and analysis of biological cells (2007–2017). *Anal. Chim. Acta* 1044:29–65
66. Chen T, Shi LZ, Zhu Q, Chandsawangbhuwana C, Berns MW. 2011. Optical tweezers and nonratiometric fluorescent-dye-based studies of respiration in sperm mitochondria. *J. Opt.* 13:044010
67. Leach J, Howard D, Roberts S, Gibson G, Gothard D, et al. 2009. Manipulation of live mouse embryonic stem cells using holographic optical tweezers. *J. Mod. Opt.* 56:448–52
68. Neuman KC, Abbondanzieri EA, Landick R, Gelles J, Block SM. 2003. Ubiquitous transcriptional pausing is independent of RNA polymerase backtracking. *Cell* 115:437–47
69. Li X, Liu C, Chen S, Wang Y, Cheng SH, Sun D. 2017. In vivo manipulation of single biological cells with an optical tweezers-based manipulator and a disturbance compensation controller. *IEEE Trans. Robot.* 33:1200–12
70. Banerjee AG, Pomerance A, Losert W, Gupta SK. 2010. Developing a stochastic dynamic programming framework for optical tweezer-based automated particle transport operations. *IEEE Trans. Autom. Sci. Eng.* 7:218–27
71. Wu Y, Sun D, Huang W, Xi N. 2013. Dynamics analysis and motion planning for automated cell transportation. *IEEE/ASME Trans. Mechatron.* 18:706–13
72. Rabaud D, Thibault P, Raven JP, Hugon O, Lacot E, Marmottant P. 2011. Manipulation of confined bubbles in a thin microchannel: drag and acoustic Bjerknes forces. *Phys. Fluids* 23:042003

73. Samandari M, Abrinia K, Sanati-Nezhad A. 2017. Acoustic manipulation of bio-particles at high frequencies: an analytical and simulation approach. *Micromachines* 8:290
74. Guo F, Mao Z, Chen Y, Xie Z, Lata JP, et al. 2016. Three-dimensional manipulation of single cells using surface acoustic waves. *PNAS* 113:1522–27
75. Li P, Mao Z, Peng Z, Zhou L, Chen Y, et al. 2015. Acoustic separation of circulating tumor cells. *PNAS* 112:4970–75
76. Naseer SM, Manbachi A, Samandari M, Walch P, Gao Y, et al. 2017. Surface acoustic waves induced micropatterning of cells in gelatin methacryloyl (GelMA) hydrogels. *Biofabrication* 9:015020
77. Ding X, Lin S-CS, Kiraly B, Yue H, Li S, et al. 2012. On-chip manipulation of single microparticles, cells, and organisms using surface acoustic waves. *PNAS* 109:11105–9
78. Velev OD, Bhatt KH. 2006. On-chip micromanipulation and assembly of colloidal particles by electric fields. *Soft Matter*. 2:738–50
79. Urbano RL, Clyne AM. 2016. An inverted dielectrophoretic device for analysis of attached single cell mechanics. *Lab Chip* 16:561–73
80. Kumemura M, Collard D, Sakaki N, Yamahata C, Hosogi M, et al. 2011. Single-DNA-molecule trapping with silicon nanotweezers using pulsed dielectrophoresis. *J. Micromech. Microeng.* 21:054020
81. Valley JK, Ohta AT, Neale SL, Hsu H-Y, Neale SL, et al. 2009. Optoelectronic tweezers as a tool for parallel single-cell manipulation and stimulation. *IEEE Trans. Biomed. Circuits Syst.* 3:424–31
82. Liu X, Shi Q, Lin Y, Kojima M, Mae Y, et al. 2018. Hydrodynamic tweezers: trapping and transportation in microscale using vortex induced by oscillation of a single piezoelectric actuator. *Sensors* 18:2002
83. Pieters RS, Tung HW, Sargent DF, Nelson BJ. 2014. Non-contact manipulation for automated protein crystal harvesting using a rolling microrobot. *IFAC Proc. Vol.* 19:7480–85
84. Leung C, Lu Z, Zhang XP, Sun Y. 2012. Three-dimensional rotation of mouse embryos. *IEEE Trans. Biomed. Eng.* 59:1049–56
85. Zhang Z, Liu J, Wang X, Zhao Q, Zhou C, et al. 2017. Robotic pick-and-place of multiple embryos for vitrification. *IEEE Robot. Autom. Lett.* 2:570–76
86. Chaumette F, Hutchinson S. 2006. Visual servo control. I. Basic approaches. *IEEE Robot. Autom. Mag.* 13:82–90
87. Hu S, Sun D. 2011. Automatic transportation of biological cells with a robot-tweezer manipulation system. *Int. J. Robot. Res.* 30:1681–94
88. Tamadazte B, Piat NLF, Dembélé S. 2011. Robotic micromanipulation and microassembly using monoview and multiscale visual servoing. *IEEE/ASME Trans. Mechatron.* 16:277–87
89. Vikramaditya B, Nelson BJ. 1997. Visually guided microassembly using optical microscopes and active vision techniques. In *Proceedings of the 1997 International Conference on Robotics and Automation*, pp. 3172–77. New York: IEEE
90. Benhimane S, Malis E. 2003. Vision-based control with respect to planar and nonplanar objects using a zooming camera. In *Proceedings of ICAR 2003: The 11th International Conference on Advanced Robotics*, pp. 991–96. New York: IEEE
91. Zhou Y, Nelson BJ. 1999. Calibration of a parametric model of an optical microscope. *Opt. Eng.* 38:1989–95
92. Ammi M, Frémont V, Ferreira A. 2009. Automatic camera-based microscope calibration for a telemicromanipulation system using a virtual pattern. *IEEE Trans. Robot.* 25:184–91
93. Jiang W, Yin Z. 2016. Seeing the invisible in differential interference contrast microscopy images. *Med. Image Anal.* 34:65–81
94. Obara B, Roberts MAJ, Armitage JP, Grau V. 2013. Bacterial cell identification in differential interference contrast microscopy images. *BMC Bioinform.* 14:134
95. Heise B, Sonnleitner A, Klement EP. 2005. DIC image reconstruction on large cell scans. *Microsc. Res. Tech.* 66:312–20
96. Sariola V, Jääskelinen M, Zhou Q. 2010. Hybrid microassembly combining robotics and water droplet self-alignment. *IEEE Trans. Robot.* 26:965–77
97. Chung SE, Dong X, Sitti M. 2015. Three-dimensional heterogeneous assembly of coded microgels using an untethered mobile microgripper. *Lab Chip* 15:1667–76

98. Steager EB, Selman Sakar M, Magee C, Kennedy M, Cowley A, Kumar V. 2013. Automated biomanipulation of single cells using magnetic microrobots. *Int. J. Robot. Res.* 32:346–59
99. Jonkman J, Brown CM. 2015. Any way you slice it—a comparison of confocal microscopy techniques. *J. Biomol. Tech.* 26:54–65
100. Wang WH, Liu XY, Sun Y. 2007. Contact detection in microrobotic manipulation. *Int. J. Robot. Res.* 26:821–28
101. Liu J, Zhang Z, Wang X, Liu H, Zhao Q, et al. 2017. Automated robotic measurement of 3-D cell morphologies. *IEEE Robot. Autom. Lett.* 2:499–505
102. Sun Y, Duthaler S, Nelson BJ. 2004. Autofocusing in computer microscopy: selecting the optimal focus algorithm. *Microsc. Res. Tech.* 65:139–49
103. Taute KM, Gude S, Tans SJ, Shimizu TS. 2015. High-throughput 3D tracking of bacteria on a standard phase contrast microscope. *Nat. Commun.* 6:8776
104. Baek YM, Tanaka S, Harada K, Sugita N, Morita A, et al. 2014. Robust visual tracking of robotic forceps under a microscope using kinematic data fusion. *IEEE/ASME Trans. Mechatron.* 19:278–88
105. Tamadazte B, Marchand E, Dembélé S, Le Fort-Piat N. 2010. CAD model-based tracking and 3D visual-based control for MEMS microassembly. *Int. J. Robot. Res.* 29:1416–34
106. Zhang Z, Dai C, Huang JY, Wang X, Liu J, et al. 2018. Robotic immobilization of motile sperm for clinical intracytoplasmic sperm injection. *IEEE Trans. Biomed. Eng.* In press. **https://doi.org/10.1109/TBME.2018.2848972**
107. Diller E, Giltinan J, Sitti M. 2013. Independent control of multiple magnetic microrobots in three dimensions. *Int. J. Robot. Res.* 32:614–31
108. Wei Y, Xu Q. 2015. An overview of micro-force sensing techniques. *Sens. Actuators A* 234:359–74
109. Jing W, Cappelleri D. 2014. A magnetic microrobot with in situ force sensing capabilities. *Robotics* 3:106–19
110. Gou X, Yang H, Fahmy TM, Wang Y, Sun D. 2014. Direct measurement of cell protrusion force utilizing a robot-aided cell manipulation system with optical tweezers for cell migration control. *Int. J. Robot. Res.* 33:1782–92
111. Jun L, Leung C, Zhe L, Yu S, Liu J, et al. 2013. Quantitative analysis of locomotive behavior of human sperm head and tail. *IEEE Trans. Biomed. Eng.* 60:390–96
112. Zhou Y, Nelson BJ, Vikramaditya B. 1998. Fusing force and vision feedback for micromanipulation. In *Proceedings of the 1998 IEEE International Conference on Robotics and Automation*, Vol. 2, pp. 1220–25. New York: IEEE
113. Dario P. 2001. PI force control of a microgripper for assembling biomedical microdevices. *IEE Proc. Circuits Devices Syst.* 148:348–52
114. Huang H, Sun D, Mills JK, Li WJ, Cheng SH. 2009. Visual-based impedance control of out-of-plane cell injection systems. *IEEE Trans. Autom. Sci. Eng.* 6:565–71
115. Seifabadi R, Rezaei SM, Ghidary SS, Zareinejad M. 2013. A teleoperation system for micro positioning with haptic feedback. *Int. J. Control. Autom. Syst.* 11:768–75
116. Onda K, Arai F. 2012. Multi-beam bilateral teleoperation of holographic optical tweezers. *Opt. Express* 20:3633–41
117. Fatikow S, Seyfried J, Fahlbusch S, Buerkle A, Schmoeckel F. 2000. Flexible microrobot-based microassembly station. *J. Intell. Robot. Syst. Theory Appl.* 27:135–69
118. Yang G, Gaines JA, Nelson BJ. 2003. A supervisory wafer-level 3D microassembly system for hybrid MEMS fabrication. *J. Intell. Robot. Syst. Theory Appl.* 37:43–68
119. Kim S, Wu J, Carlson A, Jin SH, Kovalsky A, et al. 2010. Microstructured elastomeric surfaces with reversible adhesion and examples of their use in deterministic assembly by transfer printing. *PNAS* 107:17095–100
120. Lee CH, Kim DR, Zheng X. 2010. Fabricating nanowire devices on diverse substrates by simple transfer-printing methods. *PNAS* 107:9950–55
121. Mastrangeli M, Abbasi S, Varel C, Van Hoof C, Celis JP, Böhringer KF. 2009. Self-assembly from milli- to nanoscales: methods and applications. *J. Micromech. Microeng.* 19:083001

122. Chang B, Shah A, Zhou Q, Ras RHA, Hjort K. 2015. Self-transport and self-alignment of microchips using microscopic rain. *Sci. Rep.* 5:14966
123. Donald BR, Levey CG, Paprotny I, Rus D. 2013. Planning and control for microassembly of structures composed of stress-engineered MEMS microrobots. *Int. J. Robot. Res.* 32:218–46
124. Wang H, Huang Q, Shi Q, Yue T, Chen S, et al. 2015. Automated assembly of vascular-like microtube with repetitive single-step contact manipulation. *IEEE Trans. Biomed. Eng.* 62:2620–28
125. Xu F, Wu CAM, Rengarajan V, Finley TD, Keles HO, et al. 2011. Three-dimensional magnetic assembly of microscale hydrogels. *Adv. Mater.* 23:4254–60
126. Tasoglu S, Diller E, Guven S, Sitti M, Demirci U. 2014. Untethered micro-robotic coding of three-dimensional material composition. *Nat. Commun.* 5:3124
127. Roberts KP, Bischof JC, Nelson BJ. 2003. Mechanical property characterization of mouse zona pellucida. *IEEE Trans. Nanobiosci.* 2:279–86
128. Pillarisetti A, Member S, Pekarev M, Brooks AD, Desai JP, Member A. 2007. Evaluating the effect of force feedback in cell injection. *IEEE Trans. Autom. Sci. Eng.* 4:322–31
129. Liu X, Kim K, Zhang Y, Sun Y. 2009. Nanonewton force sensing and control in microrobotic cell manipulation. *Int. J. Robot. Res.* 28:1065–76
130. Xie Y, Sun D, Liu C, Tse HY, Cheng SH. 2010. A force control approach to a robot-assisted cell microinjection system. *Int. J. Robot. Res.* 29:1222–32
131. Xu Q. 2015. Robust impedance control of a compliant microgripper for high-speed position/force regulation. *IEEE Trans. Ind. Electron.* 62:1201–9
132. Arcese L, Fruchard M, Ferreira A. 2013. Adaptive controller and observer for a magnetic microrobot. *IEEE Trans. Robot.* 29:1060–67
133. Kallio P, Ritala T, Lukkari M, Kuikka S. 2007. Injection guidance system for cellular microinjections. *Int. J. Robot. Res.* 26:1303–13
134. Wang W, Sun Y, Zhang M, Anderson R, Langille L, Chan W. 2008. A system for high-speed microinjection of adherent cells. *Rev. Sci. Instrum.* 79:104302
135. Liu J, Siragam V, Chen J, Fridman MD, Hamilton RM, Sun Y. 2014. High-throughput measurement of gap junctional intercellular communication. *AJP Hear. Circ. Physiol.* 306:H1708–13
136. Liu J, Wen J, Zhang Z, Liu H, Sun Y. 2015. Voyage inside the cell: microsystems and nanoengineering for intracellular measurement and manipulation. *Microsyst. Nanoeng.* 1:15020
137. Esteban-Fernández de Ávila B, Angsantikul P, Li J, Lopez-Ramirez MA, Ramírez-Herrera DE, et al. 2017. Micromotor-enabled active drug delivery for in vivo treatment of stomach infection. *Nat. Commun.* 8:272
138. Yim S, Gultepe E, Gracias DH, Sitti M. 2014. Biopsy using a magnetic capsule endoscope carrying, releasing, and retrieving untethered microgrippers. *IEEE Trans. Biomed. Eng.* 61:513–21
139. Filgueiras-Rama D, Estrada A, Shachar J, Castrejón S, Doiny D, et al. 2013. Remote magnetic navigation for accurate, real-time catheter positioning and ablation in cardiac electrophysiology procedures. *J. Vis. Exp.* 74:e3658
140. Li J, Li X, Luo T, Wang R, Liu C, et al. 2018. Development of a magnetic microrobot for carrying and delivering targeted cells. *Sci. Robot.* 3:eaat8829
141. Sahari A, Traore MA, Scharf BE, Behkam B. 2014. Directed transport of bacteria-based drug delivery vehicles: bacterial chemotaxis dominates particle shape. *Biomed. Microdevices* 16:717–25
142. Alapan Y, Yasa O, Schauer O, Giltinan J, Tabak AF, et al. 2018. Soft erythrocyte-based bacterial microswimmers for cargo delivery. *Sci. Robot.* 3:eaar4423
143. Dournes G, Menut F, Macey J, Fayon M, Chateil JF, et al. 2016. Lung morphology assessment of cystic fibrosis using MRI with ultra-short echo time at submillimeter spatial resolution. *Eur. Radiol.* 26:3811–20
144. Burghardt AJ, Link TM, Majumdar S. 2011. High-resolution computed tomography for clinical imaging of bone microarchitecture. *Clin. Orthop. Relat. Res.* 469:2179–93
145. Untenberger M, Tan Z, Voit D, Joseph AA, Roeloffs V, et al. 2016. Advances in real-time phase-contrast flow MRI using asymmetric radial gradient echoes. *Magn. Reson. Med.* 75:1901–8
146. Fei C, Chiu CT, Chen X, Chen Z, Ma J, et al. 2016. Ultrahigh frequency (100 MHz–300 MHz) ultrasonic transducers for optical resolution medical imagining. *Sci. Rep.* 6:28360

147. Sigrist RMS, Liau J, Kaffas AE, Chammas MC, Willmann JK. 2017. Ultrasound elastography: review of techniques and clinical applications. *Theranostics* 7:1303–29
148. Wang LV, Yao J. 2016. A practical guide to photoacoustic tomography in the life sciences. *Nat. Methods* 13:627–38
149. Masubuchi S, Morimoto M, Morikawa S, Onodera M, Asakawa Y, et al. 2018. Autonomous robotic searching and assembly of two-dimensional crystals to build van der Waals superlattices. *Nat. Commun.* 9:1413